

Electronic Supplementary Information (ESI) for Soft Matter Viscosity of Cohesive Granular Flows

Matthew Macaulay and Pierre Rognon

1 Method Details

Simulated plane shear flows

To measure the viscosity of cohesive granular flows, we used a discrete element method to simulate 10^4 adhesive grains subjected to an external constant pressure P , and shear-rate $\dot{\gamma}$. The shear cell is pseudo bi-dimensional: grains are all placed on the $x-y$ plane, but are considered to be cylinders of height d . The width of the shear cell is $100d$. Its height H is approximately $100d$; it is let free to contract or dilate to control the normal stress in the system. Shear rate and normal stress are prescribed using Lees-Edwards periodic boundaries, which act in both the x and y -directions¹. The shear rate is prescribed by moving the top and bottom boundaries in opposite directions at a velocity $v_b = \pm \frac{H}{2} \dot{\gamma}$. An external normal stress P_0 is prescribed by adjusting the cell height according to a viscous dynamics at any point in time: $\dot{H} = \frac{1}{\eta_b} (P(t) - P_0)$, where $P(t)$ is the normal stress measured in the shear cell. The viscous parameter is chosen to be with $\eta_b = 20P_0 t_i / d$, where $t_i = d \sqrt{\rho_g / P}$ is the inertial time measuring the typical time for grains to rearrange in the flow. $\eta_b \rightarrow \infty$ would correspond to a fixed volume shear. We verified that the chosen value for this parameter did not significantly affect the flow dynamics.

The discrete element method consists in integrating individual grain displacements and rotations according to Newton's second law of motion, accounting for all contact forces. With elastic grains of contact stiffness k , the shortest timescale of the system is $t_k = (m/k)^{\frac{1}{2}}$, which represents the time of contact for a binary collision excluding dissipation or adhesion. Accordingly, Newton's second laws are discretised in time (using a predictor-corrector scheme) over time steps $dt = \frac{1}{20} t_k$, which are sufficiently small to capture this time scale. After the cell height adjusted according to the predictor step, every grain position is dilated (or contracted) slightly according to in order to exactly fill the updated cell height: $y \mapsto y \times L' / L^{t-dt}$. This removes localised dilation effects near the boundary and provides more homogeneous dilation^{2,3}.

All flows are prepared by initially placing the grains without contact and then applying both the normal stress and the shear rate until a steady flow is reached. Such steady flows are characterised by a constant (albeit slightly fluctuating) system height H and internal stresses. All data shown in this paper were measured once a steady flow is established.

We quantify the homogeneity of the shear in steady flows by the following metric⁴:

$$\Delta \bar{v}_x^2 = \frac{3}{2\dot{\gamma}^2 H^3} \int_{-H}^H (\bar{v}_x(y) - y\dot{\gamma})^2 dy. \quad (1)$$

which compares the time average velocity profile $\bar{v}_x(y)$ to a linear velocity profile. A perfectly homogeneous flow leads to $\Delta \bar{v}_x = 0$ while a perfectly heterogeneous flow comprised of two blocks sliding on top of each other would lead to $\Delta \bar{v}_x = 1$. Most results presented in this paper correspond to flow with $\Delta \bar{v}_x \leq .15$. Some flows led to more heterogenous states, where a persistent shear band seemingly develops. The development of such shear bands in cohesive granular flows was previously reported in refs.⁵⁻⁷.

Grain interactions

Grains interact via pairwise contact forces. These forces are a function of the grain overlap δ , which represents an elastic deflection and is measured as the sum of two grains' radii minus their centre-to-centre distance r : $\delta = (d_i + d_j)/2 - r$. When in contact ($\delta > 0$), grains interact through the following forces: friction F^f , elastic repulsion F^e , viscous dissipation F^v , and cohesion F^c . The total interaction force \vec{F} splits into tangent \hat{n}^{\parallel} and normal \hat{n}^{\perp} directions:

$$\vec{F} = F^T \hat{n}^{\parallel} + F^N \hat{n}^{\perp}; \quad F^T = F^f; \quad F^N = F^e + F^v + F^c.$$

The elastic normal repulsion follows a Hookean linear model with a stiffness k : $F^e = k\delta$. The tangential friction between two particles in contact is modelled by an elastic tangential force capped by a sliding criteria: $F^f = \min(\frac{1}{2}k\delta; \mu_p F^e)$. The viscous dissipation is set using an equivalent coefficient of restitution of $e = \frac{1}{2}$, so that the viscous dissipation coefficient is $\alpha = -\ln(e)/(\pi^2 + \ln^2(e))^{\frac{1}{2}}$. Correspondingly, the viscous force is $F^v = \xi \dot{\delta}$ with $\xi = 2(\frac{m}{2}k)^{\frac{1}{2}} \alpha$. All simulations presented in this paper used a constant grain friction and dissipation of $\mu_p = 0.5$. The cohesion force between grains is constant $F^c = f_0$.

Adhesion models

Theories of contact mechanics have established a number of contact law for adhesive contact between elastic grains. A thorough presentation of these models can be found in refs.⁸⁻¹². We discuss here how some of the differences in contact models could be taken into account into the viscosity scaling that we proposed here.

Our analysis considers Hookean elastic contacts with constant attractive force. The DMT model¹³, which considers van der Waals interactions between two contacting spheres^{14,15}, also yields a constant attractive force f_0 which basically scales like the loss in surface energy $\Delta\gamma$ and grain size: $f_0 \propto \Delta\gamma d$. However, the DMT model considers the elastic contact between spheres described by Hertz's law, which involves a non-linear spring-like behaviour: $F^e \propto Ed^2 \left(\frac{\delta}{d}\right)^{\frac{3}{2}}$, with E being related to the Young's modulus and Poisson's ratio of the grains. This non-linearity changes the expression for the equilibrium deflection: $w_0 \propto \int_0^{\delta_{eq}} F^e(\delta) d\delta = \frac{2}{5}Ed^3(CK)^{\frac{5}{3}}$, with $K = P/E$. The corresponding cohesion-energy number is:

$$W^{DMT} \propto \frac{C^{\frac{5}{6}} K^{\frac{1}{3}}}{I}, \quad (2)$$

which is slightly different from $W = CK^{\frac{1}{2}}/I$ obtained for our Hookean contacts. A similar estimate could be performed for a JKR contact, which also involves Hertz elasticity but includes a deflection dependent adhesion force^{16–19}.

Capillary adhesion is qualitatively different. In the pendular regime, the maximum adhesion force is controlled by the water surface tension γ_w and the grain diameter: $f_0 \propto \gamma_w d^{\frac{9}{2}}$. The difference is that the attractive force has a large range. They are active until the meniscus breaks, which happens at a distance d^{rup} scaling with the grain size: $d^{rup} \propto d$. This means that the adhesion energy is not dependent on the grain stiffness. Linearising the attractive force from contact to rupture provides a first order approximation of the corresponding energy $w_0 \propto f_0 d^{rup} \propto f_0 d$. The corresponding cohesion-energy number is:

$$W^{cap} \propto \frac{C^{\frac{1}{2}}}{I}. \quad (3)$$

This qualitatively differs from grains interacting via contact adhesion, as it is independent from the grain stiffness.

2 Flow Timescales

We present here how the dimensionless numbers I , K , C and W are related to four elementary time scales: (i) the stiffness time $t_k = (\rho_g d/k)^{1/2}$ which characterises the duration of a particle collision without dissipation; (ii) the inertial time $t_i = d(\rho_g/P)^{1/2}$ which concerns the movement of a grain through on diameter under a pressure force and (iii) the shear time $t_{\dot{\gamma}} = \dot{\gamma}^{-1}$ which is the duration of one shear deformation; and (iv) The cohesion timescale $t_c = d^2(\rho_g/f_0)^{1/2}$ characterise the time for a particle to move under the force of cohesion.

I , K , C and W can be expressed by, and interpreted as combinations of these time scales. The inertial number is $I = t_i/t_{\dot{\gamma}}$, the cohesion number is $C = (t_i/t_c)^2$, the softness number is $K = (t_k/t_i)^2$, corresponding to the $P^* = K$ in Roy *et al.*²¹. The cohesion energy number is a combination of these that is independent of the inertial time $W = t_k t_{\dot{\gamma}}/t_c^2$. This reflects the fact that it is the ratio of the cohesion energy to the kinetic energy.

3 Comparison of rheological models

Several models have been devised to describe the effects of cohesion on granular rheology. Like in our study, they were determined empirically, by fitting measured friction for different levels of cohesion C , stiffness K and sometimes other parameters. We discuss here to what extent these models capture the rheological behaviour we have observed, which we proposed to model by Eq. (5) in the main text:

$$\mu(I, W) = \mu_d(I)g(W, I); \quad (4)$$

$$g(W, I) = 1 + b \frac{W}{1 + I_1/I}. \quad (5)$$

The goal of this section is to highlight what this rheology is consistent with, and what it advances in previous formulations. To facilitate comparison, we recall the two limits of our model corresponding to the cohesive-strength and cohesive-energy regime:

$$g(I \ll I_1) \approx 1 + bC \frac{K^{\frac{1}{2}}}{I_1} \quad \text{Cohesive-strength regime}; \quad (6)$$

$$g(I \gg I_1) \approx 1 + bW = 1 + bC \frac{K^{\frac{1}{2}}}{I} \quad \text{Cohesive-energy regime}. \quad (7)$$

To help with model comparison, figure 1 plots our measured function $g = \mu/\mu_d$, and how its slope $a = \frac{\partial g}{\partial C}$ decreases with the inertial number.

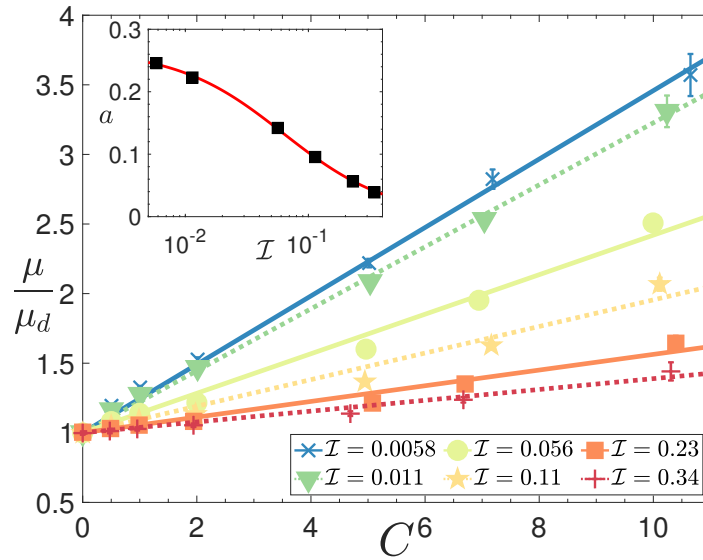


Figure 1 Measured enhancement of friction induced by cohesion (same data as in figure 2a of the paper, obtained for a fixed softness $K = 10^{-3}$). Main: $\mu/\mu_d = g$ as a function of the cohesion strength C (symbols: numerical results; line: linear fit by Eq (5)). Inset: slope $a = \frac{\partial g}{\partial C}$ as a function of the inertial number (red line fitted by $a = bK^{\frac{1}{2}}/(I + I_1)$).

Given the need for a nomenclature, in the following, we name each model by the first author of paper where they were first introduced. The model introduced in this paper is referred to as Macaulay's model.

3.1 Rognon's model

Rognon's model²² was derived from plane shear flows and flow down a slope of cohesive grains, using DTM and JKR adhesion models. In this study, the grain softness was fixed and low ($K = 10^{-5}$) and the grain coefficient of restitution was fixed. Measured friction laws were fitted by the following model:

$$\mu = \mu_{min}(C) + b(C)I, \quad (8)$$

where both functions $\mu_{min}(C)$ and $b(C)$ are linearly increasing with C . In the limit of $I = 0$, Rognon's model is consistent with Macaulay's cohesive-energy regime. However, it was derived for stiff grains, for which $C > 1$ implies $C > W = CK^{1/2}/I$. In other words, Rognon's study did not explore the cohesive energy regime. Consistently, Rognon's model does not predict the cohesive-energy rheology (Eq. 7) or the shear-induced weakening (decrease of μ with I at high cohesion numbers) captured in Macaulay's.

3.2 Roy's model

Roy's model²¹ addresses the combined effect of cohesion C and softness K . Data are captured by the following expression, which may be seen as a series of first-order corrections for each parameter that affects the friction:

$$\mu = \mu_d(I) \left(1 - \left(\frac{K}{K_0} \right)^{\frac{1}{2}} \right) (1 + aC) \quad (9)$$

$$= \mu_d(I) \left(1 + aC - \left(\frac{K}{K_0} \right)^{\frac{1}{2}} - \frac{a}{K_0^{\frac{1}{2}}} CK^{\frac{1}{2}} \right) \quad (10)$$

with constants K_0 and $a = 1.47$. It additionally includes a weakening correction for small inertial numbers and gravity effects close to a free surface, not included here. Roy's model for particle softness is based on an earlier work considering a much higher particle softness $K \leq 0.1$. Below $K < 5 \times 10^{-4}$ they find almost no effect of softness, which demarcates the stiff regime.

For relatively stiff grains such as those considered in our study, Roy's model reduces to $\mu(I, C) \approx \mu_d(I)(1 + aC)$. This is qualitatively consistent with Rognon's model, and to Macaulay's cohesive-energy regime provided the softness is fixed.

However, it does not capture the existence of the cohesive-energy regime, characterised by a coefficient a decreasing with higher inertial numbers, as shown in figure 1.

3.3 Berger's model

Berger's model²³ proposes a friction model involving the logarithm of a cohesion-modified inertial number:

$$\mu = \mu_d(I) + \frac{a_0 C}{1 - a_1 \ln(1 - I_c)}, \quad I_c = \frac{I}{(1 + a_2 C)^{\frac{1}{2}}}, \quad (11)$$

with constants a_i . It is derived from data obtained with $0 \leq C \leq 20$, $5 \times 10^{-3} \leq I \leq 0.35$ and a fixed softness. The modified inertial number I_c considers the additive stress effect of pressure and cohesion acting to confine grains. It leads to an increase in friction characterised by the function $\frac{a_0 C}{1 - a_1 \ln(1 - I_c)}$

For a given value of C , this model does predict that this term would decrease as the inertial number is increased. This is qualitatively consistent with Macaulay's cohesive-strength regime and the shear-induced weakening process. At low inertial numbers with $I_c \rightarrow 0$, this term reduces to $\frac{a_0 C}{1 + a_1 I_c}$ since $\ln(1 - I_c) \approx -I_c$. This predicts that the inertial number would also influence the friction enhancement. This does not capture the behaviour observed in Macaulay's cohesive-strength regime (Eq. 6), in which the inertial number no longer influences to the role of cohesion C on friction.

3.4 Mandal's model

The recent work in Mandal *et al.*²⁴ highlights the key role of an effective cohesion number, involving the viscous dissipation coefficient of the grains α : $C^{eff} = C^{\frac{3}{2}} K^{\frac{1}{2}} / \alpha^{\frac{1}{4}}$. They find that the inclusion of dissipation is important for yielding, however, it does not appear to be important within the flowing region^{24,25}. They demonstrate a sorting of the flow curves μ against I by the effective cohesion. Qualitatively, these results are consistent with Macaulay's observation in that a quantity resembling $CK^{\frac{1}{2}}$ drives the effect of cohesion.

Mandal's friction model consists of using C^{eff} in place of C in Berger's model (11). The observation made is that this model captures the measured friction at high inertial numbers well. However, it underestimates the friction at low inertial numbers. This is consistent with the observation that Berger's model did not capture the transition from a cohesion-energy to a cohesion-strength regime at low inertial numbers.

3.5 Gu's model

Like Berger's model, Gu's model²⁶ accounts for the effect of cohesion by an additive term to the friction law. Unlike Mandal's model, however, the effect of softness K and cohesion C are independent; there is no compound effect between the two. The model is expressed using the solid fraction ϕ as:

$$\mu = \mu_d(I) + \frac{a_0}{\left(\frac{IK^{\frac{1}{2}}}{a_1} + 1\right)^{\frac{3}{2}}} + \frac{a_2 \phi (\phi - a_3) C}{\frac{I}{a_4 C^{\frac{1}{2}}} + 1}. \quad (12)$$

The ratio in the denominator of the cohesion term $I/C^{1/2}$ corresponds to the cohesion energy term calculated in Eq. (3). Gu *et al.* similarly interpret this term as a ratio of the kinetic to cohesion energy, as for the cohesive-energy regime. Unlike the models of^{21,24} and Macaulay's model, Gu's model does not include any term involving the combined effect of cohesion and softness $CK^{\frac{1}{2}}$.

3.6 Concluding remarks

In summary, existing models appear to successfully capture either the cohesive-energy (Berger's, Mandal's, Gu's) or the cohesive-strength (Rognon's, Roy's) regimes. However, none seem to capture both. In identifying the existence of these two rheological regimes, Macaulay's model provides a way to understand the origin of their differences and to reconcile these seemingly different rheologies.

Notes and references

- [1] A. Lees and S. Edwards, *Journal of Physics C: Solid State Physics*, 1972, **5**, 1921.
- [2] M. Macaulay and P. Rognon, submitted to *Physical Review E*.
- [3] M. Macaulay and P. Rognon, *Journal of Fluid Mechanics*, 2019, **858**, year.
- [4] S. Khamseh, J.-N. Roux and F. Chevoir, *Physical Review E*, 2015, **92**, 022201.

- [5] P. Schall and M. van Hecke, *Annual Review of Fluid Mechanics*, 2010, **42**, year.
- [6] T. Divoux, M. A. Fardin, S. Manneville and S. Lerouge, *Annual Review of Fluid Mechanics*, 2016, **48**, 81–103.
- [7] E. Irani, P. Chaudhuri and C. Heussinger, *Physical review letters*, 2014, **112**, 188303.
- [8] Y. Guo and J. S. Curtis, *Annual Review of Fluid Mechanics*, 2015, **47**, 21–46.
- [9] V. Richefeu, F. Radjai and M. S. El Youssoufi, *The European Physical Journal E*, 2006, **21**, 359.
- [10] J. Tomas, *Chemical Engineering Science*, 2007, **62**, 1997–2010.
- [11] S. Luding, K. Manetsberger and J. Müllers, *Journal of the Mechanics and Physics of Solids*, 2005, **53**, 455–491.
- [12] S. Luding, *Granular matter*, 2008, **10**, 235.
- [13] B. V. Derjaguin, V. M. Muller and Y. P. Toporov, *Journal of Colloid and interface science*, 1975, **53**, 314–326.
- [14] J. R. Barber, *Contact mechanics*, Springer, 2018, vol. 250.
- [15] M. Ciavarella, J. Joe, A. Papangelo and J. Barber, *Journal of the Royal Society Interface*, 2019, **16**, 20180738.
- [16] K. L. Johnson, K. Kendall and a. Roberts, *Proceedings of the royal society of London. A. mathematical and physical sciences*, 1971, **324**, 301–313.
- [17] D. Maugis, *Journal of colloid and interface science*, 1992, **150**, 243–269.
- [18] D. Maugis, in *Contact, Adhesion and Rupture of Elastic Solids*, Springer, 2000, pp. 203–344.
- [19] S. Ji and L. Liu, *Computational Granular Mechanics and Its Engineering Applications*, Springer Singapore, Singapore, 1st edn., 2020.
- [20] N. Mitarai and F. Nori, *Advances in Physics*, 2006, **55**, 1–45.
- [21] S. Roy, S. Luding and T. Weinhart, *New journal of physics*, 2017, **19**, 043014.
- [22] P. G. Rognon, J.-N. Roux, M. Naaim and F. Chevoir, *Journal of Fluid Mechanics*, 2008, **596**, 21–47.
- [23] N. Berger, E. Azéma, J.-F. Douce and F. Radjai, *EPL (Europhysics Letters)*, 2016, **112**, 64004.
- [24] S. Mandal, M. Nicolas and O. Pouliquen, *Proceedings of the National Academy of Sciences*, 2020.
- [25] L. Staron and E. Hinch, *Granular Matter*, 2007, **9**, 205.
- [26] Y. Gu, S. Chialvo and S. Sundaresan, *Physical Review E*, 2014, **90**, 032206.